International Journal of Organizational Innovation

FORMATION OF SHEAR BANDS IN THE VICINITY OF THE DAM BODY

Tse-Shan Hsu
President, Institute of Mitigation for Earthquake Shear Banding Disasters
Professor, Feng-Chia University, Taiwan, R.O.C., tshsu@fcu.edu.tw

Yu-Chien Wu
Ph.D., Ph.D. Program for Infrastructure Planning and Engineering,
Feng-Chia University, Taiwan, R.O.C.

Zong-Lin Wu
Assistant Professor, National Chin-Yi University of Technology, Taiwan, R.O.C.

Da-Jie Lin
Associate Professor, Feng-Chia University, Taiwan, R.O.C.

Abstract

Shear bands resulting from shear banding in the vicinity of a dam body can pose a serious threat to dam safety. Therefore, the early identification of shear bands is critical during the selection of a dam site. In this study, a numerical method for identifying shear bands within a dam body is proposed, based on micro-vibration measurement results. The method is then validated using field evidence of shear bands observed at the Shi-gang Dam in Taichung, Taiwan, following the 1999 Jiji earthquake. The results demonstrate that the proposed method can accurately identify in-situ shear bands.

Keywords: shear bands, identification, micro-vibration, dam safety.

Introduction

This study conducted micro-vibration measurements at eight locations near the Shi-gang Dam, as shown in Figure 1. Points 1 through 6 are located on the right bank downstream of the dam, Point 8 is on the left bank downstream, and Point 7 is situated upstream, near the downstream side of the left-bank bridge pier of the Chang-gung Bridge.

The microtremor measurement technique developed by Wang and Wen (2023) involves recording the vertical and two horizontal components of microtremor acceleration time histories. Based on these measurements, spectral analyses can be conducted in all three directions. The details are as follows:

Figure 1. Distribution map of microtremor measurement points near the Shi-gang Dam (Google Earth, 2023).

Microtremor Time-History Curves and Spectra for Areas Adjacent to the Shi-gang Dam

Figures 2 to 4 present the ground microtremor acceleration time-history curves recorded at the first to the eight monitoring points in three directions: vertical, horizontal-1, and horizontal-2, respectively. The corresponding frequency-domain spectra, derived using the Fast Fourier Transform (FFT), are also shown.

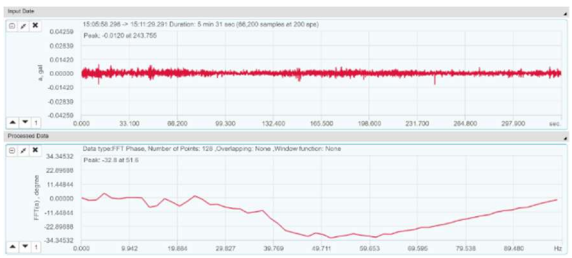

(a) The first monitoring point

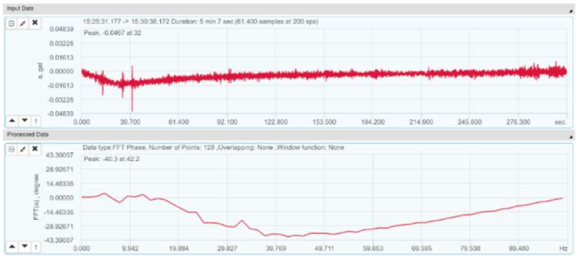

(b) The second monitoring point

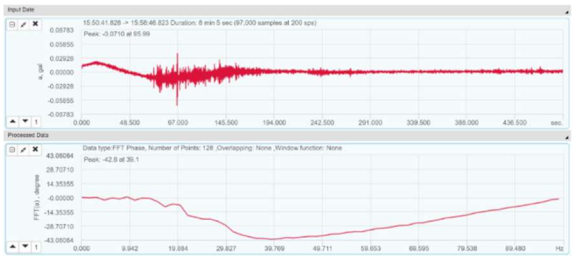

(c) The third monitoring point

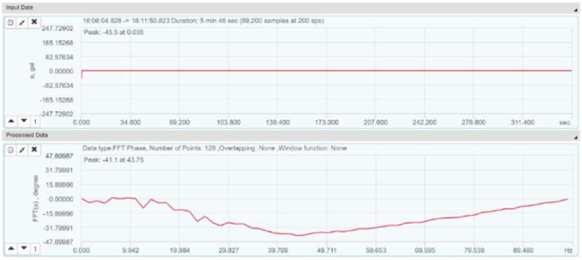

(d) The fourth monitoring point

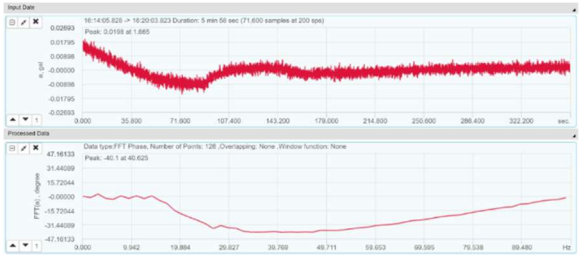

(e) The fifth monitoring point

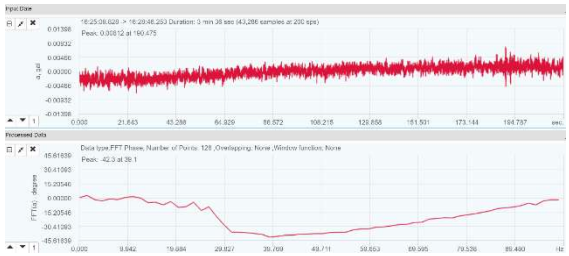

(f) The sixth monitoring point

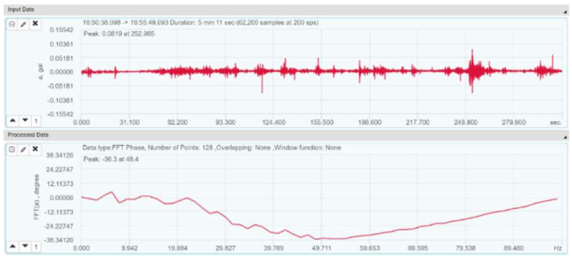

(g) The seventh monitoring point

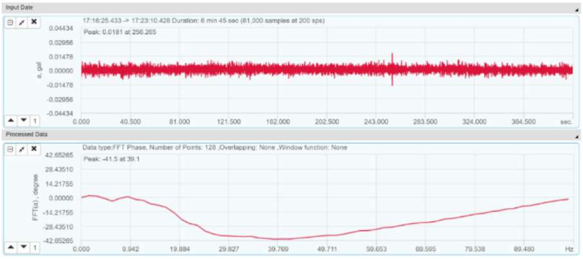

(h) The eighth monitoring point

Figure 2. The ground microtremor acceleration time-history curves recorded at the first to the eight monitoring points and the corresponding frequency-domain spectra in vertical direction.

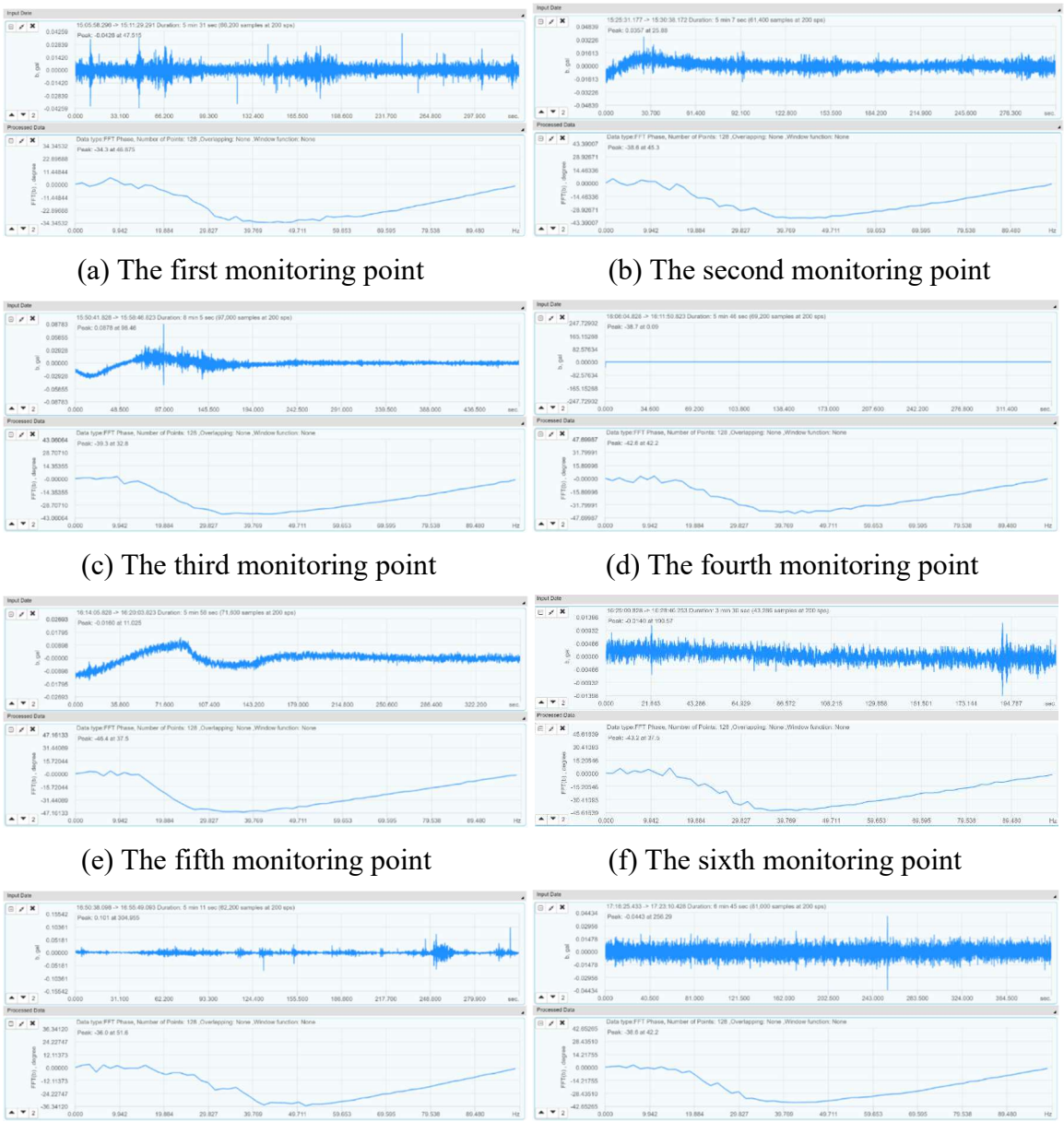

(a) The first monitoring point (b) The second monitoring point

(c) The third monitoring point (d) The fourth monitoring point

(e) The fifth monitoring point (f) The sixth monitoring point

(g) The seventh monitoring point (h) The eighth monitoring point

Figure 3. The ground microtremor acceleration time-history curves recorded at the first to the eight monitoring points and the corresponding frequency-domain spectra in horizontal-1 direction.

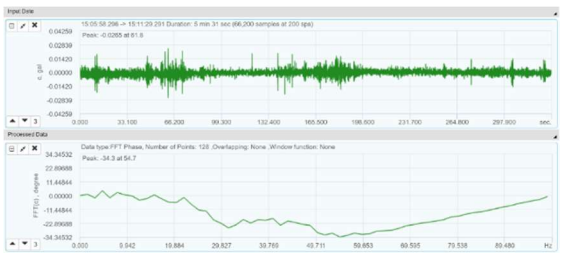

(a) The first monitoring point

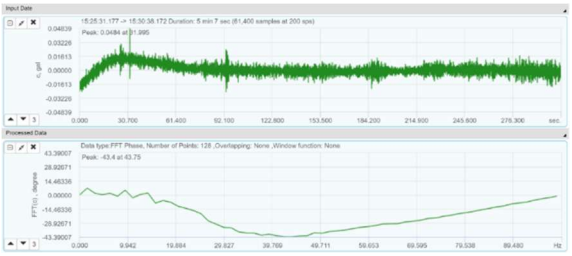

(b) The second monitoring point

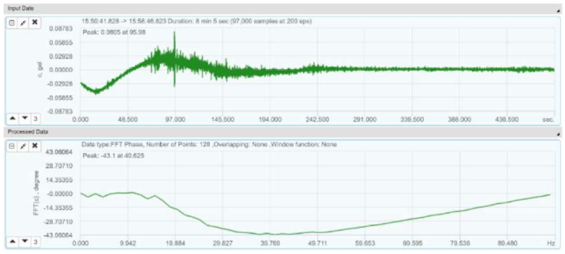

(c) The third monitoring point

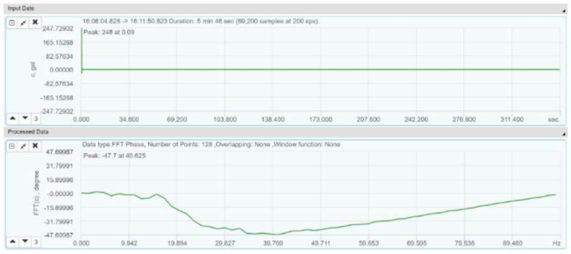

(d) The fourth monitoring point

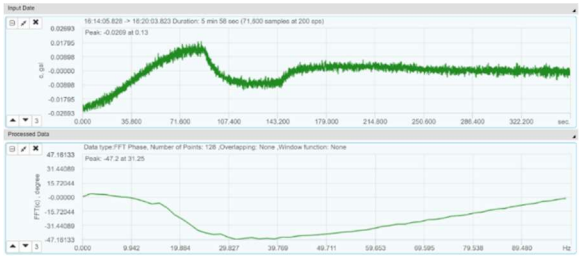

(e) The fifth monitoring point

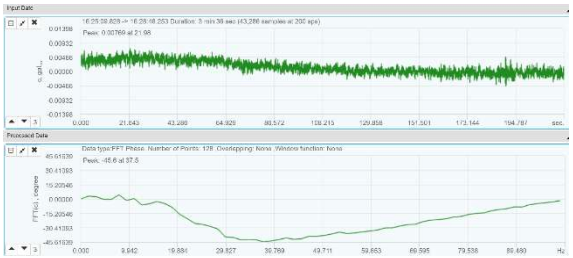

(f) The sixth monitoring point

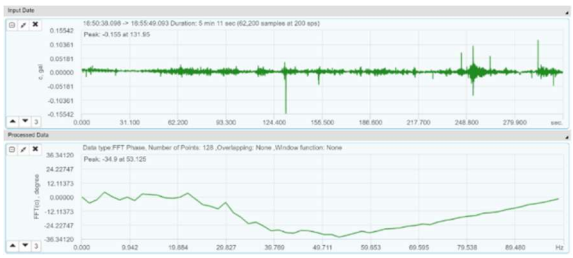

(g) The seventh monitoring point

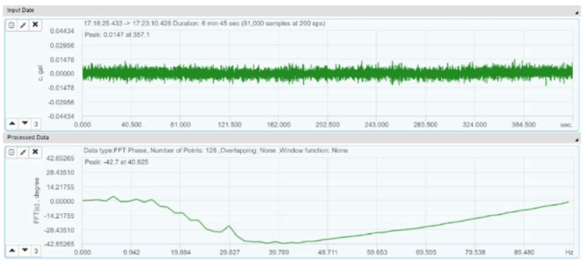

(h) The eighth monitoring point

Figure 4. The ground microtremor acceleration time-history curves recorded at the first to the eight monitoring points and the corresponding frequency-domain spectra in horizontal-2 direction.

Comparison and Discussion

For the areas near the Shi-gang Dam, Figures 2 through 4 present the spectral analysis results derived from the microtremor acceleration time-history curves measured at the eight monitoring points shown in Figure 1. Table 1 summarizes the maximum absolute values of the vertical spectral amplitude and their corresponding frequencies for the vertical, horizontal-1, and horizontal-2 directions at these eight locations.

Table 1. Maximum absolute values of the vertical component phase angle and their corresponding frequencies at the eight measurement points.

No.	Vertical Direction	Horizontal 1 direction	Horizontal 2 direction
Point 1	-32.8° (51.6Hz)	-34.3° (46.875Hz)	-34.3°(54.7Hz)
Point 2	-40.3° (42.2Hz)	-38.6° (45.3Hz)	-43.4° (43.75Hz)
Point 3	-42.6° (39.1Hz)	-39.3°(32.8Hz)	-43.1° (40.625Hz)
Point 4	-41.1° (43.75Hz)	-42.6° (42.2Hz)	-47.7°(40.625Hz)
Point 5	-47.2° (40.625Hz)	-46.4° (37.5Hz)	-40.1° (31.25Hz)
Point 6	-42.3° (39.1Hz)	-43.2° (37.5Hz)	-45.8° (37.5Hz)
Point 7	-36.3° (48.4Hz)	-36.0° (51.6Hz)	-34.9° (53.125Hz)
Point 8	-41.5° (39.1Hz)	-38.7° (42.2Hz)	-42.7° (40.625Hz)

Comparison of Maximum Absolute Phase Angle Values in the Spectra at Eight Measurement Points

For the eight monitoring points, the microtremor acceleration time-history curves are transformed into spectra with phase angles as the vertical coordinate using the Fast Fourier Transform (FFT), as shown in Figures 2 to 4. Table 1 compiles the maximum absolute phase angle values of the spectra and their corresponding frequencies for each monitoring point.

By comparing these maximum absolute phase angle values, phase angle shifts among the eight monitoring points can be identified. Similarly, by comparing the frequencies corresponding to the maximum absolute phase angles, frequency shifts between the monitoring points can be determined. The phase angle and frequency shifts observed at different measurement points within the same area are attributed to soil loosening caused by shear fault movement along the fault zone. This loosening results in increased void space in the ground due to reduced mass density, which in turn affects the wave propagation speed.

From the analysis of the maximum absolute phase angle shifts shown

in Table 2, the following results are obtained:

1. For the vertical direction, the minimum phase angle shift occurs at monitoring point 1, with a value of 32.8°, while the maximum phase angle shift occurs at monitoring point 4, with a value of 47.2°. Therefore, the maximum relative phase angle shift among the eight points is 14.4°.

2. For horizontal direction 1, the minimum phase angle shift occurs at monitoring point 1, with a value of 34.3°, and the maximum shift occurs at monitoring point 5, with a value of 46.4°. The maximum relative phase angle shift among the points is 12.1°.

3. For horizontal direction 2, the minimum phase angle shift occurs at monitoring point 1, with a value of 34.3°, while the maximum shift occurs at monitoring point 4, with a value of 47.7°. The maximum relative phase angle shift among the points is 13.4°.

Table 2. Relative offsets of spectral phase angles and frequencies among eight measurement points.

	Relative offset of the phase angle and frequency of the spectrum		
	Vertical Direction	Horizontal Direction 1	Horizontal Direction 2
Point 1-Point 5	7.5° (9.40Hz)	4.3° (1.575Hz)	9.1° (10.95Hz)
Point 2-Point 5	9.8° (12.5Hz)	5.0°(14.075Hz)	8.8° (14.075Hz)
Point 3-Point 5	8.3° (7.85Hz)	8.3° (4.675Hz)	13.4°(14.075Hz)
Point 4-Point 5	14.4° (10.975Hz)	12.1° (9.375Hz)	5.8° (23.45Hz)
Point 6-Point 5	9.5° (12.5Hz)	8.9° (9.375Hz)	11.5° (17.2Hz)
Point 7-Point 5	3.5° (3.2Hz)	1.7° (4.725Hz)	0.6° (1.575Hz)
Point 8-Point 1	8.7° (12.5Hz)	3.5° (4.675Hz)	8.4° (14.075Hz)

Comparison of Frequency Shifts Corresponding to Maximum Absolute Phase Angle Shifts

For the eight monitoring points, Table 2 lists the frequency shifts corresponding to the maximum absolute phase angle shifts for each direction (vertical, horizontal-1, and horizontal-2). The frequency shifts between the monitoring points are as follows:

1. For the vertical direction, the minimum frequency shift occurs at monitoring points 3 and 8, with a value of 39.1 Hz, while the maximum shift occurs at monitoring point 1, with a value of 51.6 Hz. The maximum relative frequency shift among the points is 12.5 Hz.

2. For horizontal direction 1, the minimum frequency shift occurs at monitoring point 3, with a value of 32.8

Hz, while the maximum shift occurs at monitoring point 7, with a value of 51.6 Hz. The maximum relative frequency shift is 18.8 Hz.

3. For horizontal direction 2, the minimum frequency shift occurs at monitoring point 7, with a value of 34.9 Hz, while the maximum shift occurs at monitoring point 1, with a value of 54.7 Hz. The maximum relative frequency shift is 19.8 Hz.

For the eight monitoring points, Table 2 lists the frequency shifts corresponding to the maximum absolute phase angle shifts for each direction (vertical, horizontal-1, and horizontal-2). The frequency shifts among the monitoring points are as follows:

1. For the vertical direction, the minimum frequency shift occurs at monitoring points 3 and 8, with a value of 39.1 Hz, while the maximum shift occurs at monitoring point 1, with a value of 51.6 Hz. The maximum relative frequency shift among the points is 12.5 Hz.

2. For horizontal direction 1, the minimum frequency shift occurs at monitoring point 3, with a value of 32.8 Hz, while the maximum shift occurs at monitoring point 7, with a value of 51.6 Hz. The maximum relative frequency shift is 18.8 Hz.

Identification of Shear Bands Using Phase Angle Shifts

When two adjacent measurement points are located respectively within a fault zone and a non-fault zone, the relative phase angle shift between them will be significant. This shift can be used to identify potential displacement along the fault zone between these points.

If δ represents the relative phase angle shift between two monitoring points, the fault displacement can be classified as follows:

- $0° < \delta \leq 5°$ corresponds to mild fault displacement.
- $5° < \delta \leq 10°$ corresponds to moderate fault displacement.
- $\delta > 10°$ corresponds to severe fault displacement.

By analyzing the relative phase angle shifts among the eight monitoring points, the fault displacement between adjacent points can be estimated, as shown in Table 3.

Table 3. Relative offsets of spectral phase angles among eight measurement points and corresponding degrees of shear banding.

	Vertical Direction	Horizontal Direction 1	Horizontal Direction 2
Point 2-Point 1	7.5° (medium)	4.3°(slight)	9.1°(medium)
Point 3-Point 1	9.8°(medium)	5.0°(slight)	8.8°(medium)
Point 4-Point 1	8.3°(medium)	8.3° (medium)	13.4°(high)
Point 5-Point 1	14.4°(high)	12.1°(high)	5.8° (medium)

Point 6-Point 1	9.5°(medium)	8.9°(medium)	11.5°(high)
Point 7-Point 1	3.5°(slight)	1.7°(slight)	0.6°(slight)
Point 8-Point 1	8.7°(medium)	3.5°(slight)	8.4° (medium)

Identification of Shear Bands Using Frequency Shifts

The relative frequency shifts between two monitoring points can also be used to identify fault displacements. If Δ represents the relative frequency shift, the fault displacement can be classified as follows:

- $0\ \text{Hz} < \Delta \leq 10\ \text{Hz}$ corresponds to mild fault displacement.
- $10\ \text{Hz} < \Delta \leq 20\ \text{Hz}$ corresponds to moderate fault displacement.
- $\Delta > 20\ \text{Hz}$ corresponds to severe fault displacement.

Using the relative frequency shifts among the eight monitoring points (as shown in Table 4), the fault displacement between adjacent points can be estimated.

Table 4. Relative offsets of spectral frequencies among eight measurement points and corresponding degrees of shear banding.

	Vertical Direction	Horizontal Direction 1	Horizontal Direction 2
P2-P1	9.40Hz (slight)	1.575Hz (slight)	10.95Hz (medium)
P3-P1	12.5Hz (medium)	14.075Hz (medium)	14.075Hz (medium)
P4-P1	7.85Hz (slight)	4.675Hz (slight)	14.075Hz (medium)
P6-P1	10.975Hz (medium)	9.375Hz (slight)	23.45Hz (high)
P7-P1	12.50Hz (medium)	9.375Hz (slight)	17.20Hz (medium)
P8-P1	3.20Hz (slight)	4.725Hz (slight)	1.575Hz (slight)

Verification of Physical Shear Banding

During the 1999 Jiji earthquake, fault movement associated with shear bands caused uneven uplift of the Shigang Dam's right bank, as shown in Figure 5, resulting in severe structural damage. Additionally, lateral shear banding led to transverse fractures in the dam structure, as illustrated in Figure 6.

Figure 5. The shear banding triggered significant uplift, resulting in damage to the Shi-gang Dam.

Figure 6. Horizontal shear banding observed at Shi-gang Dam

Additionally, downstream of Shi-gang Dam, shear banding induced brittle fractures in the riverbed, resulting in localized deep scouring, as shown in Figure 7.

Figure 7. Downstream Riverbed of Shi-gang Dam After Channel Deepening (Google Earth, 2023)

At the time of site selection, Shi-gang Dam was located within a low-vibration zone as designated by the government, which set the horizontal seismic coefficient at $k_h = 0.1$. However, during the dam's design phase, a higher horizontal seismic coefficient of $k_h = 0.15$ was adopted, along with a vertical seismic coefficient of $k_v = 0.075$. The design considered the Sanyi fault—located 4.5 km from the dam—as the controlling fault (see Figure 8).

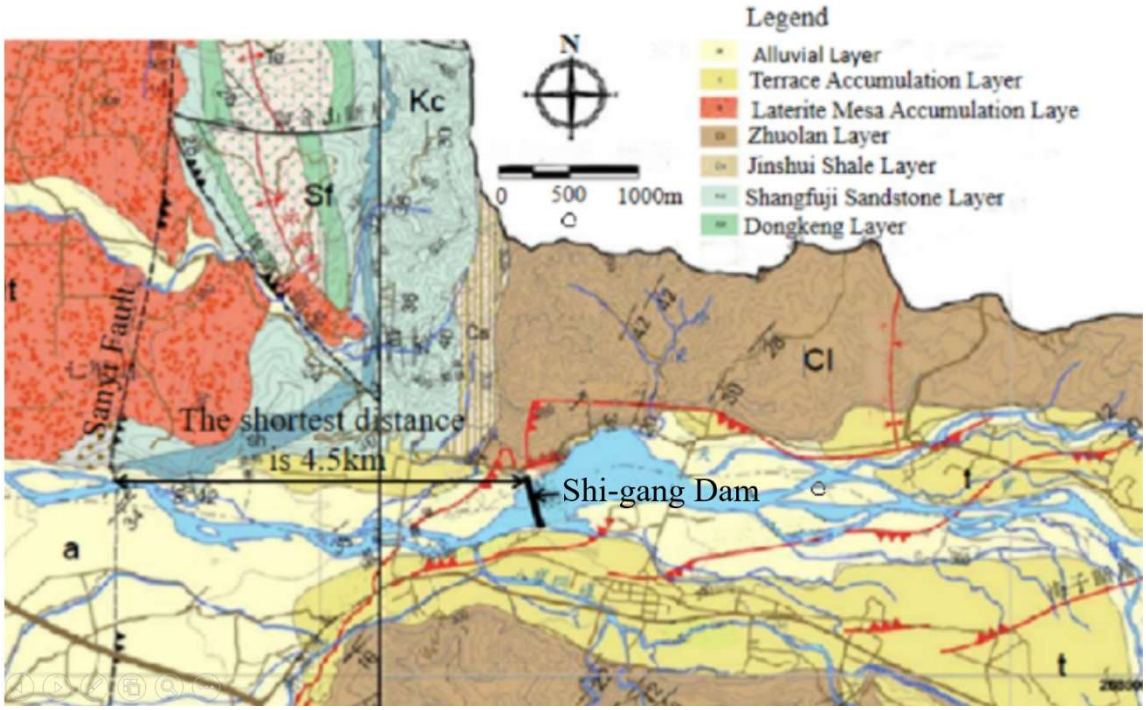

Figure 8. The shortest distance from Shi-gang Dam to the Sanyi Fault (Hsu, 2010).

Before the Jiji earthquake, the Chulinpu Fault (see Figure 9) existed near the Shi-gang Dam and underwent significant shear banding during the 1999 earthquake, causing damage to the dam.

Following the Jiji earthquake, seismic design codes emphasized ground vibration protection, with the San-Yi fault clearly crossing the Shi-gang Dam. The shortest rupture distance (r_{rup}) between the dam and the fault should theoretically be 0 km. However, during the emergency repair work post-earthquake, the peak ground acceleration (PGA) calculated using the attenuation formula for the dam site was infinite when r_{rup} = 0 km, though the actual horizontal PGA applied in the repair project was finite.

Figure 10 shows that the maximum width of the upstream riverbed is 755 m, while the downstream riverbed narrows to 240 m. This narrowing corresponds to fault-induced displacement features in the region near Shi-gang Dam.

Figure 11 reveals a high density of triangular facets on the slopes near the dam. These triangular facets are indicative of displaced landform features, thus confirming the significant shear banding effects near the dam.

Figure 12(a) illustrates the presence of interwoven fault zones and

fault structures, including principal displacement shear (D), thrust shear (P), Riedel shear (R), conjugate Riedel shear (R'), and compression textures (S). Figure 12(b) further shows that these shear bands and shear textures intersect the microtremor monitoring points (1 to 8) selected for this study.

Figure 9. The Chelongpu Fault Exists in the Vicinity of Shi-gang Dam (Google Earth, 2023).

Figure 10. Current Status of Shi-gang Dam (Google Earth, 2023).

Figure 11. Dense shear bands on the north slope of Shi-gang Dam
(Google Earth, 2023)

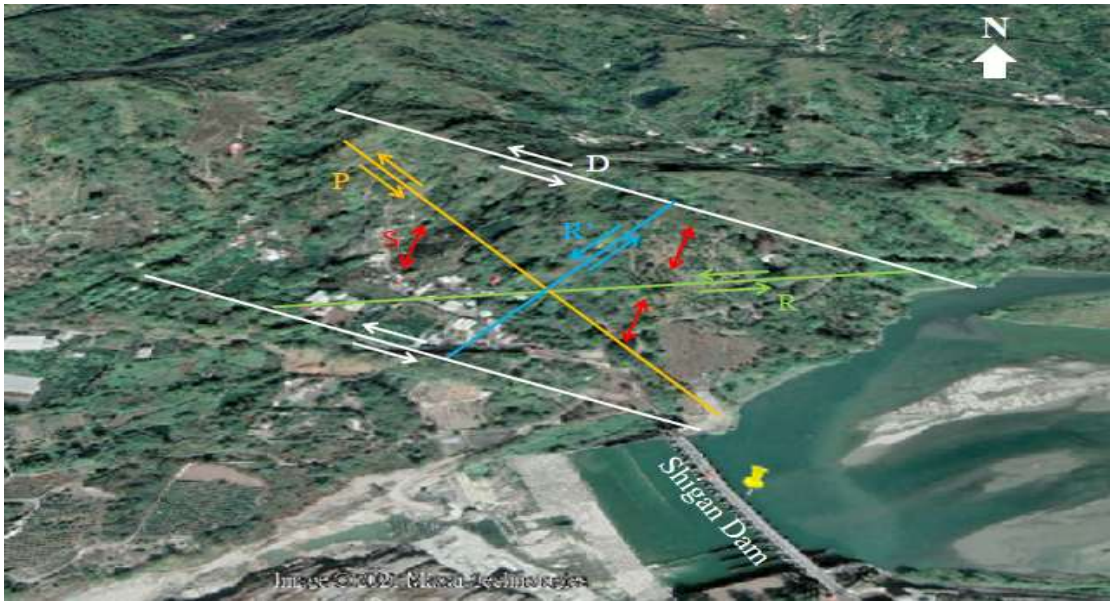

(a) Right bank slopes of Shi-gang Dam

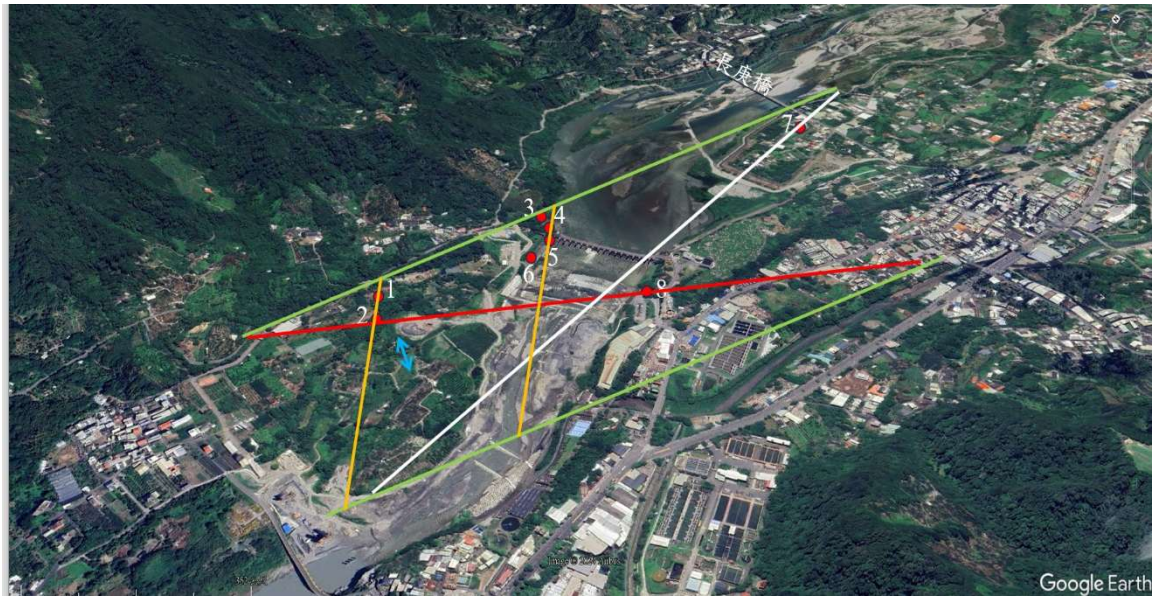

(a) Shear bands and shear textures occurring along the range from measuring point 1 to measuring point 8.

Figure 12. Shear bands and shear textures in the vicinity of Shi-gang Dam (Google Earth, 2023).

Therefore, the shear bands and shear textures identified through satellite imagery and shear banding features around Shi-gang Dam, as shown in Figure 12, validate the findings of this study. The microtremor measurements and FFT spectral analysis conducted at the monitoring points, along with the observed relative phase angle and frequency shifts, correspond closely with the shear banging characteristics documented during the 1999 Jiji earthquake.

Conclusions and Recommendations

The findings of this study corroborate that, alongside the existing qualitative methods for shear band identification documented in the literature, the present paper introduces a novel quantitative approach based on field surface micro-vibration measurements. A salient feature of this proposed methodology is its capacity to quantitatively categorize shear banding into slight, moderate, and severe levels, thereby facilitating a more nuanced and objective assessment in future applications. Consequently, the implementation of this approach holds considerable potential to enhance risk mitigation strategies for structural failures, exemplified by the catastrophic events during the earthquake in Turkey on February 6, 2023.

References

Google Earth, Website: http://www.google.com.tw/intl/zh-TW/earth/, 2023

Hsu, Tse-Shan, "A Study on the Distribution of Pre-Existing Shear Bands in Reservoirs and Corresponding Design and Reinforcement Methods." A Research Report Commissioned by the Central Region Water Resources Office, Water Resources Agency, Ministry of Economic Affairs, 2010

Wang, Hongjun, and Y-E Wen, "Research on Micro Vibration Measurement and Analysis Method of Using," *Metrology Science and Technology*, Vol. 67, No. 6, pp. 44-48, 2023`